Meteoritics & Planetary Science 37, 449–457 (2002)
Available online at http://www.uark.edu/meteor

Hornblende alteration and fluid inclusions in Kärdla impact crater, Estonia: Evidence for impact-induced hydrothermal activity

KALLE KIRSIMÄE[1,2]*, STEN SUUROJA[3], JUHO KIRS[1], AULIS KÄRKI[4], MAILE POLIKARPUS[1], VÄINO PUURA[1] AND KALLE SUUROJA[3]

[1]Institute of Geology, University of Tartu, Vanemuise 46, 51014 Tartu, Estonia
[2]Institute of Geography, University of Tartu, Vanemuise 46, 51014 Tartu, Estonia
[3]Geological Survey of Estonia, Kadaka tee 80/82, 12618 Tallinn, Estonia
[4]Department of Geosciences, University of Oulu, P.O. Box 333, FIN-90571 Oulu, Finland
*Correspondence author's e-mail address: arps@ut.ee

(Received 2000 December 1; accepted in revised form 2001 December 17)

Abstract–The well-preserved Kärdla impact crater, on Hiiumaa Island, Estonia, is a 4 km diameter structure formed in a shallow Ordovician sea ~455 Ma ago into a target composed of thin (~150 m) unconsolidated sedimentary layer above a crystalline basement composed of migmatite granites, amphibolites and gneisses. The fractured and crushed amphibolites in the crater area are strongly altered and replaced with secondary chloritic minerals. The most intensive chloritization is found in permeable breccias and heavily shattered basement around and above the central uplift. Alteration is believed to have resulted from convective flow of hydrothermal fluids through the central areas of the crater. Chloritic mineral associations suggest formation temperatures of 100–300 °C, in agreement with the most frequent quartz fluid inclusion homogenization temperatures of 150–300 °C in allochthonous breccia. The rather low salinity of fluids in Kärdla crater (<13 wt% $NaCl_{eq}$) suggests that the hydrothermal system was recharged either by infiltration of meteoric waters from the crater rim walls raised above sea level after the impact, or by invasion of sea water through the disturbed sedimentary cover and fractured crystalline basement. The well-developed hydrothermal system in Kärdla crater shows that the thermal history of the shock-heated and uplifted rocks in the central crater area, rather than cooling of impact melt or suevite sheets, controlled the distribution and intensity of the impact-induced hydrothermal processes.

INTRODUCTION

Most impact cratering studies have focused on the processes of crater formation; consequently, far less is known about the post-impact crater evolution. Post-impact hydrothermal alteration of crater rocks is a common impact-related phenomenon, which can provide insight into crater formation and development. Formation of hydrothermal systems in impact craters results from the large amount of kinetic energy released to the target. Propagation of supersonic shock wave into the target and projectile causes extraordinarily high pressures and temperatures reaching, respectively, >100 GPa and >3000 °C in large-scale impacts (Melosh, 1989). Adiabatic decompression of projectile and target rocks compressed above ~45 GPa during shock wave passage may lead to their melting and vaporization (Stöffler, 1972). Strong differential temperatures in the crater basement due to the post-shock residual heat remaining in rocks after decompression creates a hydrothermal circulation system if water is present at the crater site or it can be also fed by fluids formed during degassing of impact melt in large craters such as Ries (Newsom *et al.*, 1986).

Impact-induced hydrothermal activity, although poorly studied, is known in many terrestrial craters (*e.g.*, Allen *et al.*, 1982; Newsom *et al.*, 1986; Komor *et al.*, 1988; Koeberl *et al.*, 1989; Masaitis and Naumov, 1993; Boer *et al.*, 1996; McCarville and Crossey, 1996; Sturkell *et al.*, 1998; Naumov, 1999; Gibson and Reimold, 2000) and implied for extraterrestrial craters as well (Allen *et al.*, 1982; Newsom *et al.*, 1996). Except for the Lockne (Sturkell *et al.*, 1998) and Roter Kamm craters (Koeberl *et al.*, 1989; Reimold *et al.*, 1997), impact-induced hydrothermal activity is accompanied by a cooling of the impact melt bodies or suevites. Signs for an occurrence of an impact melt sheet and/or suevite have not been found in the Kärdla. Moreover, the coptogenic fragmental breccias that constitute the crater filling allochthonous deposits contain <1 vol% melted material (Puura *et al.*, 2000). We present data on the alteration of hornblende in amphibolitic target rocks and of secondary fluid inclusions in impact

breccias, both of which indicate a short-lived, yet well-developed, hydrothermal system formed in the brecciated and heated crater basement after impact.

LOCATION AND GEOLOGICAL SETTING

The Kärdla impact crater is located on the island of Hiiumaa, 25 km off the northwestern coast of Estonia. The crater is 4 km in diameter and ~540 m deep with a central uplift exceeding 100 m high (Fig. 1). The Kärdla crater formed in a shallow (<100 m deep) epicontinental Ordovician sea ~455 Ma ago into a target composed of a 150 m thick early Paleozoic siliciclastic and carbonate sedimentary sequence covering a crystalline basement (Puura and Suuroja, 1992). Although the diameter of the Kärdla crater is the same as the transition diameter between simple and complex, the presence of an uplift suggests a structurally complex impact crater. Plado *et al.* (1996) has suggested that the presence of seawater on top of the target facilitated the formation of the central uplift.

The Paleoproterozoic crystalline basement, representing a 1.7–2.0 Ga old Svecofenninan crustal segment (Gorbatchev and Bogdanova, 1992), is composed of regionally metamorphosed amphibolite-facies migmatitic granites and quartz-feldspar gneisses with amphibolites, biotite gneisses and biotite-amphibole gneisses. Amphibolitic rocks constitute up to 30% of all rock types.

The well-preserved crater depression is filled with autochthonous and allochthonous coptogenic fragmental breccias (including slumped and fallback fragmental breccias) covered by resurge conglomerates, conglomeratic turbidites and sands that were eroded from uplifted crater walls prior to burial by carbonate sediments (Puura and Suuroja, 1992). Carbonates also comprise the upper part of the crater depression filling (Fig. 1). Autochthonous breccias are composed of cataclastic crystalline basement rocks which are fractured to different degrees. Fracturing decreases gradually with depth and extends to ~1 km beneath the original surface. The porosity of the shock-affected rocks decreases from ~18% in impact

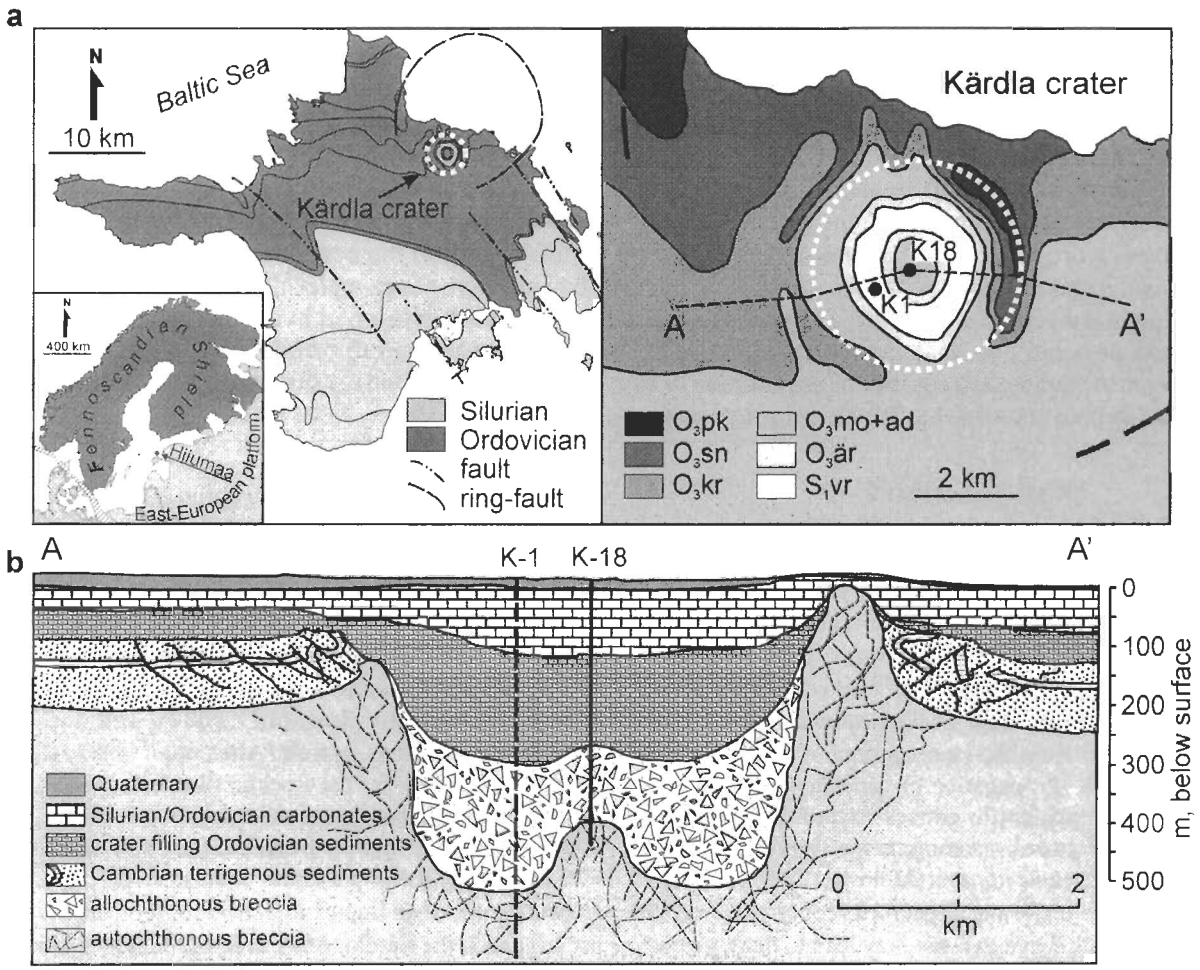

FIG. 1. Simplified geological map of Hiiumaa Island and of Kärdla crater area (a), and cross-section of the crater in a west-east direction with the location of the drill cores studied (b). Legend: O_3pk = Upper Ordovician Paekna Formation, O_3sn = Saunja Formation, O_3kr = Kõrgesaare Formation, O_3mo+ad = Moe and Adila Formation, $O_3är$ = Ärina Formation, S_1vr = Lower Silurian Varbola Formation. White dashed line shows location of Kärdla crater.

breccias to ≤5% in the fractured basement at a depth of 815 m (Plado *et al.*, 1996). Allochthonous fragmental breccias of different generations consist of a polymict mixture of crystalline and sedimentary rock fragments. Amphibolitic rocks occur within autochthonous breccias as fractured and displaced blocks. The amphibolitic rock fragments in allochthonous breccias occur as clasts of various sizes in the fine-grained breccia matrix. In the crater area the fractured and crushed amphibolites are strongly altered, being often totally replaced by secondary mineral phases.

MATERIAL AND METHODS

A total of 18 samples of altered amphibolite inclusions from the allochthonous fragmental breccia sequence and crushed amphibolite rocks from the autochthonous breccias, and 12 fluid inclusion samples from the upper part of autochthonous fragmental breccias in the crater depression were taken from drill-cores K-1 and K-18 (Figs. 1 and 2). Drill-core K-1 penetrates the whole section of the allochthonous and autochthonous breccias inside the crater up to 815 m depth below ground surface. Drill-core K-18 opens section of the allochthonous breccias in central part of the crater and reaches the slightly brecciated crystalline rocks of central peak (depths 399–432 m).

Minerals in the original host rock and their alteration products were studied by x-ray diffractometry (XRD), optical microscopy, scanning electron microscopic (SEM) back-scattered electron images and semiquantitative energy dispersive spectrometer analysis (EDS).

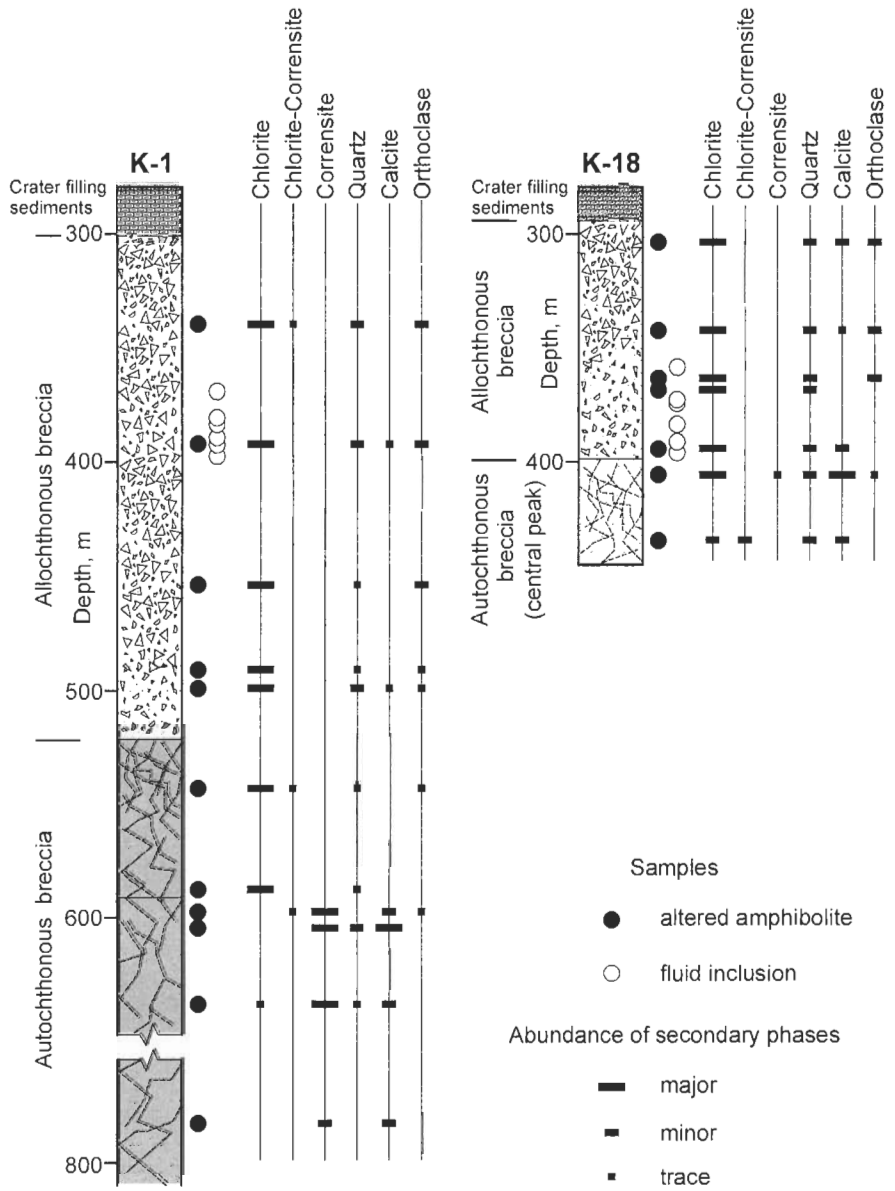

FIG. 2. Schematic lithological profiles of the drill-cores K-1 and K-18 with the location of samples and distribution of the secondary mineral abundances.

For XRD analysis, the whole-rock powder and oriented <2 μm clay fractions were used. Oriented clay fractions were analysed in the air-dried state and after treatment with ethylene glycol (EG). Diffraction patterns were recorded using a DRON 3M diffractometer, with Ni-filtered CuKα radiation, and step scanning at 0.02° 2θ steps for 3 and 5 s for oriented preparations and random powders, respectively.

SEM studies were performed with a JEOL 6300 SEM equipped with Oxford ISIS EDS at the Oulu University, Finland. Digital x-ray images of Ca, K, Na, Mg and Mn were collected and also qualitative line analyses over zones of different compositions were collected and examined.

Microthermometry on fluid inclusions in quartz was measured in thin sections by standard techniques of heating and freezing (Roedder, 1984) using a modified MKS-2 heating-cooling stage at the Institute of Precambrian Geology and Geochronology, Russian Academy of Sciences, St. Petersburg.

RESULTS

Hornblende Petrography

The hornblende abundance in autochthonous breccias varies between 5 and 60 vol%. The amphibolites have a massive and

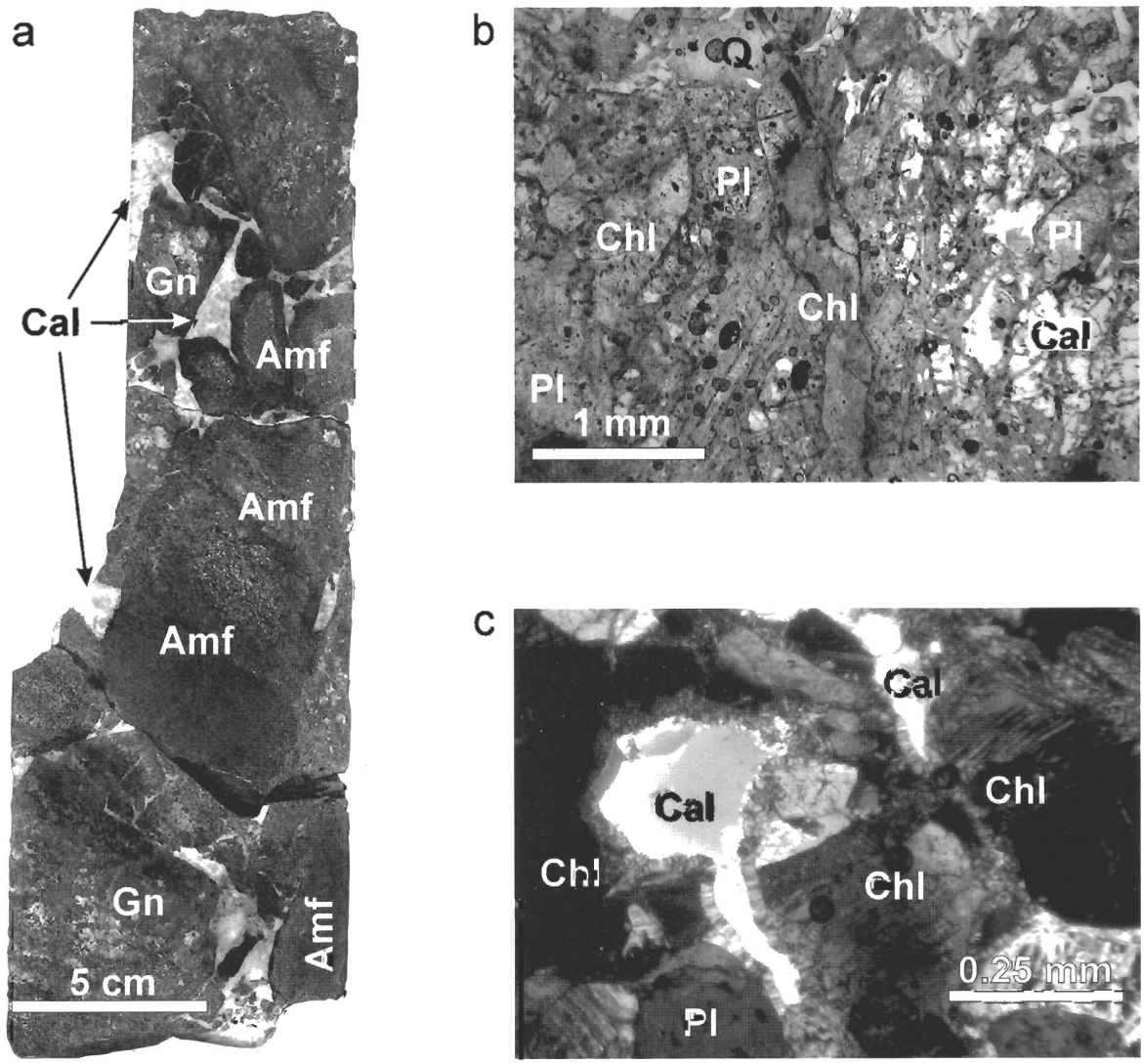

FIG. 3. Polished rock sample and photomicrographs of altered amphibolites at Kärdla. (a) Crushed amphibolite and gneiss clasts with calcite lined fractures and cavities. Note the alteration fronts inside the clasts. Drill-core K-18, depth 301 m; (b) altered amphibole replaced by chlorite and secondary calcite and quartz with plagioclase relics replaced mainly by K-feldspar. Amphibole crystals are completely altered to chlorite, but original elongated prismatic outlines of hornblende crystals are still observable. Plane polarized light. Drill-core K-18, depth 398.4 m; (c) radially oriented chlorite crystallites growing into a pore space filled by secondary calcite. Crossed polars. Drill-core K-18, depth 398.4 m. Amf = amphibolite, Gn = gneiss, Cal = calcite, Chl = chlorite, Pl = altered plagioclase, Q = quartz.

locally linear fabric with unevenly spaced fractures filled with secondary calcite aggregates. Green hornblende consists of isometric or elongated prismatic grains between 0.5 and 2 mm in length. Optical mineralogic analysis suggests a hastingsitic composition of the hornblende. Planar deformation features (PDFs) are missing, but mineral grains are usually fractured and crushed into smaller pieces. Generally, the hornblende grains are replaced with chlorite aggregate, but linear fabric of elongated hornblende crystals is still observable (Fig. 3).

Allochthonous fragmental breccias contain only ~5 vol% of hornblende. Hornblende grains are severely crushed and predominately replaced by a fine-grained submicroscopic mass of secondary chlorite, quartz, Fe-oxides and calcite. Cavities and fractures between amphibolite clasts are filled with calcite (rarely dolomite), quartz, K-feldspar and minor sulphides (mainly pyrite) and goethite (Fig 3).

Scanning Electron Microscopy

SEM and SEM-EDS examination shows that hornblende has been replaced by fine-grained Fe-Mg rich silicate (chlorite, corrensite) and silica (quartz) (Fig. 4). Areas composed only of silica (quartz) consist of irregular patches with angular edges in a fine-grained chlorite crystallite matrix, indicating authigenic quartz precipitation in the form of individual crystals and/or secondary overgrowths. The Al-, Mg- and Fe-rich fine-grained mass of submicron crystallites which fill most of the former hornblende area is interpreted to be chlorite and/or corrensite. High-magnification SEM images of the chloritic masses in allochthonous breccia matrix show the typical euhedral platy clay mineral morphology of chlorite crystallites.

X-Ray Diffraction

Examples of the whole-rock powder XRD patterns of amphibolites are shown in Fig. 5 and the distribution of the secondary phases in the drill cores in Fig. 2. The major alteration products of hornblende in amphibolite rock fragments were identified as trioctahedral chlorite, mixed-layered chlorite-smectite (corrensite) and corrensite-chlorite type phases. The samples also contain quartz, K-feldspar and albite, calcite, Fe-oxyhydrates, relic biotite and traces of hornblende (Figs. 2 and 5). Amphibolitic clasts within fall-back breccias have been completely replaced by chlorite and/or mixed-layered chlorite-corrensite phases, secondary quartz, K-feldspar, calcite, and rarely dolomite. In the fractured basement rocks and autochthonous breccias, the hornblende has been replaced by trioctahedral chlorite and chlorite-corrensite type interstratified phases. The maximum alteration of hornblende occurs in alteration haloes surrounding the calcite-filled veins in the upper part of the crater floor and central peak. Macroscopically unaltered and weakly altered amphibole in this section is significantly altered to mixed-layered chlorite-smectite (corrensite) type phase. Chlorites are Ib(β97°) polytypes characterized by a single

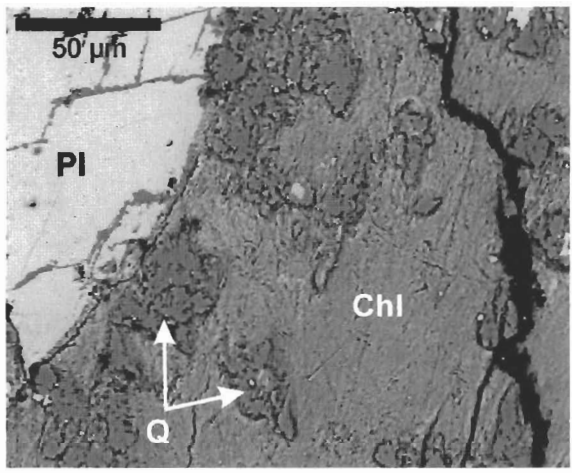

FIG. 4. SEM photomicrograph of altered hornblende grain in contact with unaltered plagioclase in autochthonous breccia in drill-core K-1, depth 603.4 m. Chl = chlorite and/or corrensite, Pl = plagioclase, Q = quartz.

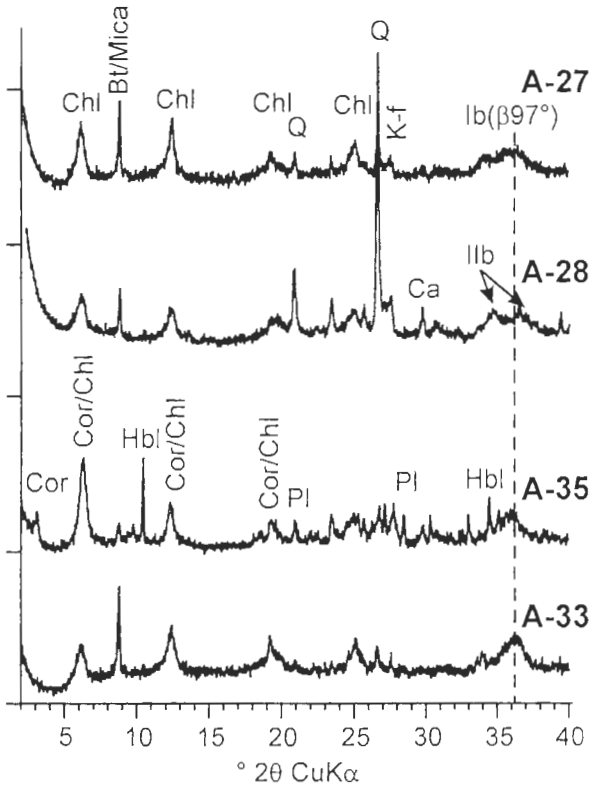

FIG. 5. Representative XRD patterns of the amphibolite whole-rock unoriented powder preparations. Samples A-27 and A-28 represent amphibolitic fragments in allochthonous breccia at depths 496 and 500 m of drill-core K-1, respectively, whereas A-33 and A-35 are from amphibolite fragments in autochthonous breccia at depths 588 and 597 m, respectively. Chl = chlorite, Cor-Chl = chlorite-corrensite, Cor = corrensite, Bt/Mica = biotite and/or K-mica, Hbl = hornblende, Q = quartz, Pl = plagioclase, K-f = K-feldspar, Ca = calcite. Ib(β97°), IIb = characteristic lines of the chlorite polytypes.

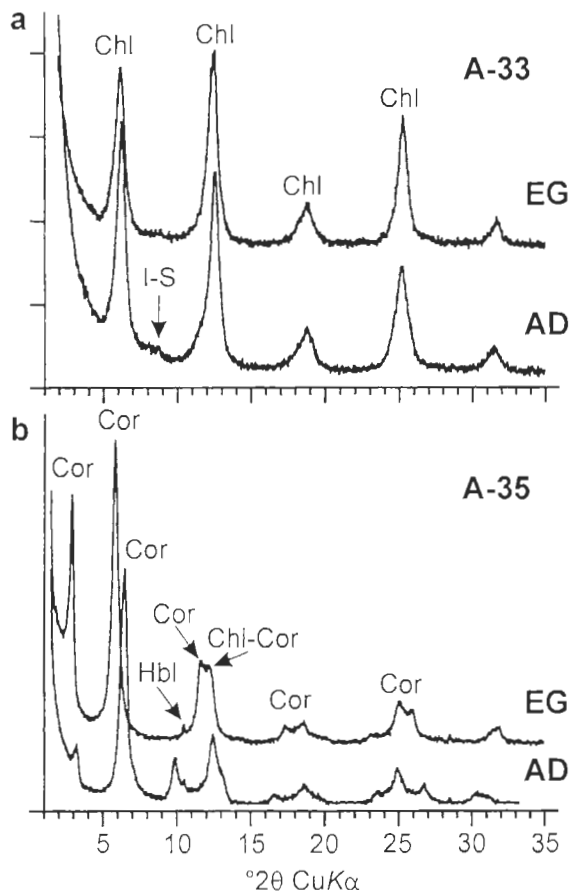

FIG. 6. Representative XRD patterns of the <2 μm fraction in air dry (AD) and in ethylene glycol (EG) solvated state. (a) Sample A-33 from drill-core K-1, depth 588 m. (b) Sample A-35 from drill-core K-1, depth 597 m. Chl = chlorite, I-S = illite-smectite, Cor = corrensite, Chl-Cor = chlorite-corrensite.

strong, but broad peak at 2.47 Å (Fig. 5). Only 1 sample out of 18 revealed a IIb polytype together with the dominant Ib(β97°) type. The Ib(β90°, 97°) polytype chlorites are usually Fe-rich compared to IIb type metamorphic chlorites (Curtis *et al.*, 1985).

The clay fractions (<2 μm) contain mixed-layered chlorite (corrensite and corrensite-chlorite) and discrete Fe-rich chlorite minerals (Fig. 6). The presence of a 50:50 chlorite-smectite (corrensite) mixed-layer phase is confirmed by superstructure d(001) spacing expansion from 29 Å in air-dried state to 31.1 Å in EG saturated state (Fig. 6b). Heating of the corrensite-rich sample at 500 °C for 1 h caused the spacing to collapse to 24 Å. The slight Fe-rich chlorite peak shift towards higher d-spacings and a peak broadening after EG solvation (Fig. 6a) probably reflects the presence of chlorite-corrensite type phase in chlorite rich samples. The XRD patterns of samples from the autochthonous breccia sequence show the presence of a mixed-layer illite-smectite, which also either have a hydrothermal origin or, most probably, reflect highly illitic illite-smectite, the most abundant clay mineral in the Lower Cambrian clayey sediments (Kirsimäe *et al.*, 1999), which formed the thickest part (~100 m) of the sedimentary target at the impact event.

Fluid Inclusions

Fluid inclusions (Fig. 7) were measured in fractured single-crystal quartz and granitic rock fragments in allochthonous fragmental breccias. The size of the fluid inclusions typically vary from 2 to 10 μm, rarely up to 20–30 μm. The inclusions are most frequent in quartz grains without any visible shock features and in quartz where the fluid inclusion trails crosscut the PDFs. In rare cases grains of yellowish-grey quartz were identified with up to four sets of decorated PDFs with gaseous single-phase fluid inclusions along PDF planes. The composition of the fluid inclusions is predominantly aqueous ($NaCl$-H_2O), but rare H_2O-CO_2 ($NaCl$-H_2O-CO_2) or CO_2 composition fluids were also found.

These fluid inclusions were most probably formed by impact-generated hydrothermal solutions. High temperatures (>400 °C)—which are much higher than the decrepitation temperatures of fluid inclusions—and particularly high pressures (>10 GPa) during PDF formation in quartz (Grieve *et al.*, 1996) exclude the survival of primary fluid inclusions. In addition, the fluid inclusion trails, which crosscut the planar elements, show that they postdate the impact event. This confirms that the entrapped fluids are impact related. Similar conclusion based on the relationship between fluid inclusion trails and PDF systems have been drawn by Komor *et al.* (1988), Koeberl *et al.* (1989) and Boer *et al.* (1996) for the Siljan, Roter Kamm and Manson impact craters, respectively.

The results of homogenization temperature (T_h) measurements of the quartz fluid inclusions encompass a wide range from 110 to 440 °C, with the maximum peak between 150 and 300 °C (Fig. 8). This temperature range is similar to the T_h values obtained for fluid inclusions in quartz found in Siljan (Komor *et al.*, 1988), Roter Kamm (Koeberl *et al.*, 1989) and in the Manson impact structures (Boer *et al.*, 1996). Trapping temperatures (T_t) are estimated assuming that pressures during entrapment were due to the overburden of

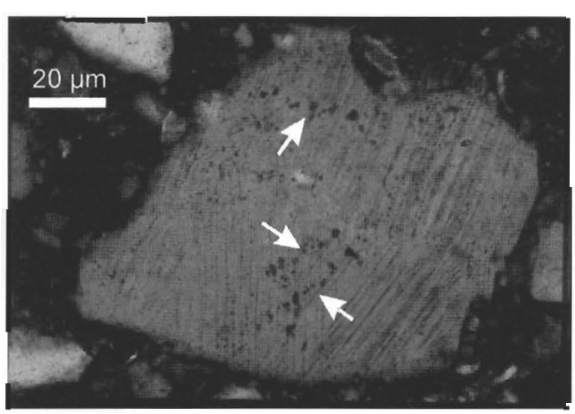

FIG. 7. Photomicrograph (crossed polars) of fluid inclusions in a quartz grain with three sets of PDFs in allochthonous breccia. K-1 drill-core, depth 383 m. Arrows indicate fluid inclusion trails crosscutting PDFs.

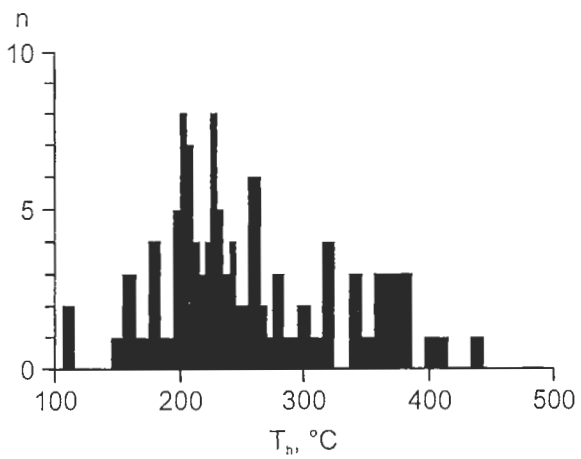

FIG. 8. Histogram of the aqueous (H_2O-NaCl) quartz fluid-inclusion homogenisation temperatures (T_h) in allochthonous breccia unit in Kärdla crater.

porous and unconsolidated fall-back and resurge breccias and hence, nearly equal to the hydrostatic pressure. Consequently, the pressure corrections are negligible and minimum T_t values are about 230–350 °C for the most common inclusions with most frequent T_h. The final ice melting temperatures of inclusions range from –9.1 to –0.3 °C with a maximum at –3 °C, which reflect fluid salinities between 13 and 0.8 wt% $NaCl_{eq}$, with most samples ≤5wt% $NaCl_{eq}$ (Bodnar, 1993). The aqueous fluid inclusions are NaCl dominated, although the melting behaviour of some inclusions suggests a few $CaCl_2$ ($CaCl_2$-NaCl-H_2O) inclusions.

DISCUSSION AND CONCLUSIONS

The formation of secondary clay minerals and particularly of Fe-smectite (saponite), corrensite and chlorite in impact-hosted hydrothermal systems is described in Allen *et al.* (1982), Phinney *et al.* (1978), Komor *et al.* (1988), McCarville and Crossey (1996), and Naumov (1999). Chloritization of mafic minerals (hornblende, pyroxene) begins with the formation of saponite type smectite, which in progressive hydrothermal alteration transforms to corrensite (Reynolds, 1988). Corrensite, however, can form directly under hydrothermal conditions at temperatures between ~100 and 200 °C (Inoue and Utada, 1991), whereas the upper limit of corrensite thermal stability lies at 220–225 °C (Tómasson and Kristmannsdóttir, 1972). The next stage in corrensite-to-chlorite conversion is the growth of chlorite layers in corrensite to form discrete chlorite domains in a corrensite matrix (Beaufort *et al.*, 1997). Hayes (1970) concluded from studies of sedimentary chlorites that the natural polytype progression with increasing temperature is Ib_d – Ib(β97°) – Ib(β90°) – IIb(β97°) with the temperature for the Ib–IIb transition to be about 150–200 °C. Thus, the prevalence of the Ib(β97°) polytype and the rarity of the IIb polytype in the Kärdla samples would suggest fluid temperatures of ≤200 °C. However, Walker (1993) showed that the Ib polytypes can be stable up to 300 °C and IIb polytype may possibly form at temperatures as low as 50 °C. Nevertheless, Inoue (1995) states that trioctahedral Fe-chlorite appears ubiquitously in the higher-grade alteration zones where the temperature exceeded 200 °C in alkaline or neutral solutions and at ~300 °C chlorite starts to react with illite and/or K-feldspar to form biotite. Therefore we propose that maximum temperatures of 200–300 °C were reached during hydrothermal alteration (widespread Fe-chlorite formation) of the amphibolite rocks in the upper part of the autochthonous breccias and in amphibolitic clasts including in the allochthonous breccias in the central crater area. Chloritization intensity decreases with decreasing fracturing downward into the crater floor, where chlorite occurs only in immediate proximity to the fracture planes and corrensite prevails within macroscopically unaltered amphibolite blocks, indicating maximum temperatures below 200 °C.

The temperature range estimated from the alteration assemblage is in good agreement with the most frequent quartz fluid inclusion homogenization temperatures (150–300 °C) in the allochthonous breccia. The temperature range of fluid inclusion homogenization (110 to 440 °C) probably reflects the temperature evolution in the central part of the hydrothermal system developed in the Kärdla crater. The highest fluid-inclusion trapping temperatures were about 400–500 °C directly after the crater formation. However, the absence of the high-temperature hydrothermal mineral assemblages (*e.g.*, garnet-actinolite-epidote) suggests that the initial high-temperature stage (>300 °C) was too short for alteration to achieve equilibrium phases. The most intense fluid-inclusion entrapment and the hydrothermal alteration occurred at lower temperatures (100–300 °C) resulting in the chloritization of amphibole. Precipitation of calcite (rarely dolomite) in veins and cavities reflects probably the final stages of the cooling, when the temperature reached ambient conditions.

The most frequent PDF orientations in quartz are along the $\{10\bar{1}3\}$ and $\{10\bar{1}2\}$ planes (our unpublished data), pointing a shock stage Ib (Grieve *et al.*, 1996) for the rocks at Kärdla crater. This corresponds to a shock pressure range of 20–35 GPa and post-shock temperatures of about 170–300 °C (Grieve *et al.*, 1996), which well agrees with the temperatures suggested by secondary minerals and fluid inclusion data. In the central part of the crater depression, however, the high-temperature (>300 °C) fluid inclusions suggest higher initial post-shock temperatures. Also, the localization of the most intensive chloritization in fall-back and resurge breccias around and above the shattered rocks of the central uplift indicates that the hydrothermal fluids were driven by convective passage and discharge through the most heated central peak area of the crater (Fig. 9). However, the approximate stratigraphic uplift of the central peak in Kärdla crater is ≤1 km, which would have added a maximum of only 35–40 °C assuming a geothermal gradient of 25–30 °C km^{-1} and average surface temperature of 10 °C. Therefore, the shear heating during formation of the central

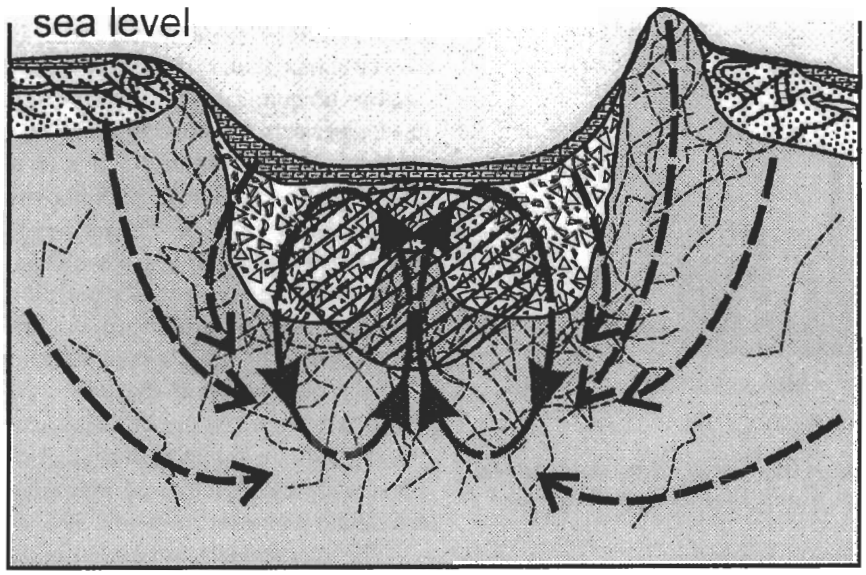

FIG. 9. Schematic reconstruction of the short-lived impact-induced hydrothermal system at Kärdla crater. Striped area shows the zone with the maximum alteration. Dashed arrows indicate water infiltration pathways and solid arrows show probable location of the post-impact hydrothermal system.

uplift and the rapid unloading of the target basement likely provided an additional thermal impulse into this area, which initiated the hydrothermal fluids movement (Masaitis and Naumov, 1993; Crossey *et al.*, 1994). A similar post-impact hydrothermal system within a central uplift was described in the ~80 km diameter Puchezh–Katunki impact crater (Naumov, 1999) and in the 35 km diameter Manson crater (Boer *et al.*, 1996). Although scale and the amounts of energy released in these impacts are considerably different, both exhibit similar post-impact hydrothermal alteration patterns. Therefore, it is reasonable to expect the same spatially limited hydrothermal processes in all other terrestrial and, presumably, in extraterrestrial complex impact craters, providing that water is present.

The low salinity of fluid inclusions is usually interpreted as indicative of hydrothermal circulation feed by meteoric waters, whereas high salinity solutions are thought to be related to the fluid release during silicate rock melting (*e.g.*, Koeberl *et al.*, 1989). The rather low salinity of fluids in Kärdla crater (<13 wt% of $NaCl_{eq}$, most ≤5 wt% $NaCl_{eq}$) suggests that the hydrothermal system was recharged either by infiltration of meteoric waters from the crater rim walls raised above sea level after the impact, or by infiltration of seawater (3.0–3.5 wt% $NaCl_{eq}$) through the disturbed sedimentary cover and fractured crystalline basement (Fig. 9).

The maintenance time of such hydrothermal systems may be few hundred years to several tens of thousand years for small- to large-size craters (Onorato *et al.*, 1978; McCarville and Crossey, 1996; Newsom *et al.*, 1996) and up to 2 Ma for the largest terrestrial craters (Ivanov and Deutsch, 1999). The hydrothermal system in Kärdla crater could last for several hundreds of years, given its moderate size, high water/rock ratios, absence of distinctive impact melt sheet and involvement of both conductive and convective cooling mechanisms.

In conclusion, we propose that the formation of fluid inclusions and the hornblende degradation proceeded by corrensite-to-chlorite transformation in Kärdla impact crater is related to the development of a local, probably short-lived, hydrothermal system in the crater depression immediately after the crater formation in a shallow (<100 m) seabed. Temperatures of the hydrothermal waters recorded by fluid inclusions and mineral associations range from 100 to 300 °C. The fluid inclusion data suggest the initial temperatures of the hydrothermal fluids were up to about 100–200 °C higher, but the temperature decline to ~300 °C was probably rapid, and the high-temperature hydrothermal mineral assemblage was not formed. The hydrothermal system was possibly driven by thermal convection of low salinity (≤5 wt% $NaCl_{eq}$) meteoric or sea water through the crater central peak area. The high-temperature conditions, extensive fluid exchange and, consequently, the high-rate pervasive hydrothermal alteration processes existed probably for only a relatively short time of several hundred years. Although the well-developed hydrothermal system in Kärdla crater is unrelated to the cooling of impact melt or suevite bodies, it shows similarity with hydrothermal systems in large, impact-melt rich craters. The thermal history of the shock heated and uplifted rocks in the central crater area, rather than of melt or suevite sheets, controls the distribution and intensity of these impact-induced hydrothermal processes.

Acknowledgments–The work was supported in part by Estonian Science Foundation grants ESF-4417 and ESF-4541, and by Research Theme TBGGG-1826. The samples were provided by Estonian

Geological Survey. We are grateful to A. Bushmin and E. Ljapin, Institute of Precambrian Geology and Geochronology, RAS, St. Peterburg for help with fluid inclusion analyses. Robert Szava-Kovats, Department of Applied Ecology, University of Tartu is thanked for valuable comments and language improvement. We sincerely thank Associate Editor Alexander Deutsch, Laura Crossey and Roger L. Gibson for constructive and thoughtful reviews of the paper.

Editorial handling: A. Deutsch

REFERENCES

ALLEN C. G., GOODING J. L. AND KEIL K. (1982) Hydrothermally altered impact melt rock and breccia: Contributions to the soil of Mars. *J. Geophys. Res.* **87**, 10 083–10 101.

BEAUFORT D., BARONNET A., LANSON B. AND MEUNIER A. (1997) Corrensite: A single phase or a mixed-layer phyllosilicate in the saponite-to-chlorite conversion series? A case study of Sancerre-Couy deep drilling hole (France). *Am. Mineral.* **82**, 109–124.

BODNAR R. J. (1993) Revised equation and table for determing the freezing-point depressions of H_2O-NaCl solutions. *Geochim. Cosmochim. Acta* **57**, 683–684.

BOER R. H., REIMOLD W. U., KOEBERL C. AND KESLER S. E. (1996) Fluid inclusion studies on drill core samples from the Manson impact crater: Evidence for post-impact hydrothermal activity. In *The Manson Impact Structure, Iowa: Anatomy of an Impact Crater* (eds. C. Koeberl and R. R. Anderson), pp. 377–382. GSA Spec. Paper **302**, Geological Society of America, Boulder, Colorado, USA.

CROSSEY L. J., KUDO A. M. AND MCCARVILLE P. (1994) Post-impact hydrothermal systems: Manson impact structure, Manson, Iowa (abstract). *Lunar Planet. Sci.* **25**, 299–300.

CURTIS C. D., HUGHES C. R., WHITEMAN J. A. AND WHITTLE C. K. (1985) Compositional variation within some sedimentary chlorites and some comments on their origin. *Mineral. Mag.* **49**, 375–386.

GIBSON R. L. AND REIMOLD W. U. (2000) Deeply exhumed impact structures: A case study of the Vederford Structure, South Africa. In *Impacts and the Early Earth* (eds. I. Gilmour and C. Koeberl), pp. 249–277. Lec. Notes Earth Sci. **91**, Springer, Berlin, Germany.

GORBATCHEV R. AND BOGDANOVA S. (1992) Frontiers in the Baltic Shield. *Precambrian Res.* **64**, 3–21.

GRIEVE R. F., LANGENHORST F. AND STÖFFLER D. (1996) Shock metamorphism of quartz in nature and experiment: II. Significance in geoscience. *Meteorit. Planet. Sci.* **31**, 6–35.

HAYES J. B. (1970) Polytypism of chlorite in sedimentary rocks. *Clays Clay Miner.* **18**, 285–306.

INOUE A. (1995) Formation of clay minerals in hydrothermal environments. In *Origin and Mineralogy of Clays* (ed. B.Velde), pp. 268–330. Springer-Verlag, Berlin, Germany.

INOUE A. AND UTADA M. (1991) Smectite-to-chlorite transformation in thermally metamorphosed volcanoclastic rocks in the Kamikita area, northern Honshu, Japan. *Am. Mineral.* **76**, 628–640.

IVANOV B. AND DEUTSCH A. (1999) Sudbury impact event: Cratering mechanics and thermal history. In *Large Meteorite Impacts and Planetary Evolution II* (eds. B. O. Dressler and V. L. Sharpton), pp. 389–397. GSA Spec. Paper **339**, Geol. Soc. America, Boulder, Colorado, USA.

KIRSIMÄE K., JØRGENSEN P. AND KALM V. (1999) Low temperature diagenetic illite-smectite in Lower Cambrian clays in North Estonia. *Clay Min.* **34**, 151–163.

KOEBERL C., FREDRIKSSON K., GÖTZINGER M. AND REIMOLD W. U. (1989) Anomalous quartz from the Roter Kamm impact crater, Namibia: Evidence for post-impact activity? *Geochim. Cosmochim. Acta* **53**, 2113–2118.

KOMOR S. C., VALLEY J. W. AND BROWN P. E. (1988) Fluid-inclusion evidence for impact heating at the Siljan Ring, Sweden. *Geology* **16**, 711–715.

MASAITIS V. L. AND NAUMOV M. V. (1993) Puchezh–Katunki astrobleme: Preliminary model of hydrothermal circulation system (abstract). *Meteoritics* **28**, 390–391.

MCCARVILLE P. AND CROSSEY L. J. (1996) Post-impact hydrothermal alteration of the Manson impact structure. In *The Manson Impact Structure, Iowa: Anatomy of an Impact Crater* (eds. C. Koeberl and R. R. Anderson), pp. 347–376. GSA Spec. Paper **302**, Geological Society of America, Boulder, Colorado, USA.

MELOSH H. J. (1989) *Impact Cratering. A Geologic Process*. Oxford Univ. Press, New York, New York, USA. 245 pp.

NAUMOV M. V. (1999) Hydrothermal-metasomatic mineralization (in Russian). In *Deep Drilling at Puchezh-Katunki Impact Crater* (eds. V. L. Masaitis and L. A. Pevzner), pp. 276–286. VSEGEI, St. Peterburg, Russia.

NEWSOM H. E., GRAUP G., SEWARDS T. AND KEIL K. (1986) Fluidization and hydrothermal alteration of the suevite deposit at the Ries crater, West Germany, and implications for Mars. *Proc. Lunar Planet. Sci. Conf.* **17th**; *J Geophys. Res.* **91**, E239–E251.

NEWSOM H. E., BRITTELLE G. E., HIBBITTS C. A., CROSSEY L. J. AND KUDO A. M. (1996) Impact crater lakes on Mars. *J. Geophys. Res.* **101**, 14 951–14 956.

ONORATO P. I. K., UHLMANN D. R. AND SIMONDS C. H. (1978) The thermal history of the Manicouagan impact melt sheet, Quebec. *J. Geophys. Res.* **83**, 2789–2799.

PHINNEY W. C., SIMONDS C. H., COCHRAN A. AND MCGEE P. E. (1978) West Clearwater, Quebec impact structure, part II: Petrology. *Proc. Lunar Planet. Sci. Conf.* **9th**, 2659–2694.

PLADO J., PESONEN L. J., ELO S., PUURA V. AND SUUROJA K. (1996) Geophysical research on the Kärdla impact structure, Hiiumaa Island, Estonia. *Meteorit. Planet. Sci.* **31**, 289–298.

PUURA V. AND SUUROJA K. (1992) Ordovician impact crater at Kärdla, Hiiumaa Island, Estonia. *Tectonophysics* **216**, 143–156.

PUURA V., KÄRKI A., KIRS J., KIRSIMÄE K., KLEESMENT A., KONSA M., NIIN M., PLADO J., SUUROJA K. AND SUUROJA S. (2000) Impact-induced replacement of plagioclase by K-feldspar in granitoids and amphibolites at the Kärdla Crater, Estonia. In *Impacts and the Early Earth* (eds. I. Gilmour and C. Koeberl), pp. 417–445. Lec. Notes Earth Sci. **91**, Springer, Berlin, Germany.

REIMOLD W. U., KOEBERL C. AND BRANDT D. (1997) Suevite at the Roter Kamm impact crater, Namibia. *Meteorit. Planet. Sci.* **32**, 431–437.

REYNOLDS R. C., JR. (1988) Mixed-layer chlorite minerals. *Rev. Miner.* **19**, 601–629.

ROEDDER E. (1984) Fluid inclusions. *Rev. Miner.* **12**, 1–644.

STÖFFLER D. (1972) Deformation and transformation of rock-forming minerals by natural and experimental shock processes: I. Behavior of minerals under shock compressions. *Fortschr. Mineral.* **49**, 50–113.

STURKELL E. F. F., BROMAN C., FORSBERG P. AND TORSSANDER P. (1998) Impact-related hydrothermal activity in the Lockne impact structure, Jamtland, Sweden. *Eur. J. Mineral.* **10**, 589–606.

TÓMASSON J. AND KRISTMANNSDÓTTIR H. (1972) High temperature alteration minerals and thermal brines, Reykjanes, Iceland. *Contrib. Mineral. Petrol.* **36**, 123–134.

WALKER J. R. (1993) Chlorite polytype geothermometry. *Clays Clay Miner.* **41**, 260–267.